Low-temperature silica-rich gold mineralisation in mafic VMS systems: evidence from the Troodos ophiolite, Cyprus

Andrew J. Martin[1,2*], Iain McDonald[1], Katie A. McFall[1], Christopher J. MacLeod[1] and Hazel M. Prichard[1+]

[1]School of Earth and Ocean Sciences, Cardiff University, UK

[2]Department of Earth Sciences, Memorial University of Newfoundland, CANADA

[*]Corresponding author: ajmartin@mun.ca

[+] Deceased

Abstract

The Troodos ophiolite Cyprus hosts the on-land analogue for mafic, Cu-rich, or Cyprus-type VMS deposits. In addition to high-temperature (>350˚C) sulfide mound related mineralisation, other fossil seafloor mineralising systems are known to operate, including those characterised by an enrichment in Au and abundant silicification. In this study the mineralogy and geochemistry of four Au and silica-rich localities in Troodos are considered, these include: Kokkinovounaros, Mathiatis South, Touronjia and Alpen Rose. We present whole rock geochemical and mineralogical data characterising the distribution of Au in the off-axis hydrothermal system of Troodos.

Samples from silica-rich localities have two distinct sample mineralogies: supergene samples that contain predominantly goethite, hematite and jarosite and hypogene samples that contain quartz, amorphous silica and minor hematite. Hypogene samples from Mathiatis South and Kokkinovounaros are enriched in Au with a median concentration of 1.5 ppm relative to supergene samples that contain 0.1 ppm (n = 107). This indicates that Au enrichment occurred on the seafloor and is not solely related to supergene weathering processes in silica-rich mineralisation.

We suggest that silica-rich Au mineralisation in Troodos formed during the migration of newly formed crust off-axis or as white smokers proximal to known VMS deposits. In off-axis silica-rich mineralisation, Au was probably remobilised from shallow crustal reservoirs during the low-temperature fluid flow in the lower extrusive sequence as the crust cooled and migrated off-axis.

Based on modern seafloor analogues, we propose a revised model for the off-axis hydrothermal system that explains the distribution of Au in silica-rich mineralisation. We suggest that mineralisation formed an intermediary between high-temperature (350°C) on-axis VMS deposits and the low-temperature silicification of umbers (<150°C).

Introduction

Off-axis hydrothermal systems

Gold is an element widely associated with seafloor sulfide mineralisation in a range of tectonic settings (Hannington et al. 1991; Melekestseva et al. 2017; Mercier-Langevin et al. 2011; Moss and Scott 2001). Volcanogenic Massive Sulfide (VMS) deposits associated with the Troodos ophiolite are generally Au-poor (Hannington et al. 1998; Mercier-Langevin et al. 2011); however, previous studies have shown that Au may be concentrated in low-temperature "off-axis" silicified umbers (Prichard and Maliotis 1998). In these systems silicification postdates VMS formation and formed distally to the spreading axis as the crust cooled and migrated off-axis (Prichard and Maliotis 1998). It remains unclear for how long and how far spatially off-axis hydrothermal circulation remained active in Troodos, as low-temperature hydrothermal activity is reported for 20–30 km off-axis in active seafloor spreading environments (Honorez et al. 1981). In active seafloor hydrothermal systems, black smoker vent sites characterise only the active, high-temperature portion of the hydrothermal system with extinct sulfide accumulations preserved distally but within a few km of the spreading axis.

In this study we investigate a mineralisation style that is silica-rich and sulfide-poor that occurs distally to known VMS deposits. Four mineralised localities are considered that display different mineralogical, morphological and geochemical characteristics compared to a typical Troodos VMS deposit. Historically, studies by Prichard and Maliotis (1998) have indicated that Au enrichment is associated with silicification in umbers, however, the temperature and source of Au in these systems remains poorly constrained. This study aims to characterise the source, distribution and enrichment of Au in VMS and silica-rich mineralisation of the Troodos ophiolite to better understand the mobility of metals during low-temperature off-axis fluid circulation.

The Troodos ophiolite

The exceptionally exposed Late Cretaceous (~92 Ma: Mukasa and Ludden 1987) Troodos ophiolite of Cyprus hosts the type locality for Cyprus-type, mafic or Cu-Zn VMS deposits (e.g., Adamides 2010; Galley et al. 2007; Hannington et al. 1998). The exact tectonic origin of the Troodos ophiolite remains controversial and it is now widely accepted that Troodos formed in a supra-subduction environment, most likely a nascent fore-arc type setting (Miyashiro 1973; Pearce and Robinson 2010). The domical uplift of Troodos has led to the exposure of a complete oceanic pseudostratigraphy with the mantle section surrounded radially by cumulate and plutonic rocks, the sheeted dyke complex (SDC), the extrusive sequence, consisting of a transitional basal group horizon (BG) between the SDC and lavas, and the upper and lower pillow lavas (UPL-LPL) (Gass 1980, 1968; Fig. 1).

The SDC are locally altered to greenschist facies alteration assemblages (e.g., epidote) indicating high-temperature (>350°C) fluid-rock interaction during hydrothermal alteration (Gass and Smewing 1973). Moreover, it is widely accepted that the SDC contributed metals to the overlying hydrothermal system during VMS formation (i.e. spilite and epidosite formation; Jowitt et al. 2012; Patten et al. 2016, 2017).

The spreading structure of Troodos suggests crustal accretion akin to processes recognised at intermediate to slow-spreading ridges (Escartin and Canales 2011). The formation of regional-scale graben structures indicate tectonic stretching, thinning and rotation of the upper crust during seafloor spreading (Varga and Moores 1985; Fig. 1). Three regional-scale grabens that are thought to represent fossil seafloor spreading ridges are preserved on the northern flank of Troodos (Varga and Moores 1985; Fig. 1). From west to east these are: Solea, Mitsero and Larnaca grabens. Spreading relationships between grabens suggest that both Solea and Mitsero could have formed in an “off-axis” position i.e. through the faulting of older crust in a ridge flank type setting (van Everdingen and Cawood 1995; Hurst et al. 1994). VMS deposits and silicified umbers are spatially associated with these seafloor structures (Constantinou and Govett 1973; Prichard and Maliotis 1998).

Off-axis silicification

Previous studies have identified areas distal to high-temperature VMS mineralisation that contain elevated Au concentrations (>1 ppm) associated with silicified Mn and Fe-rich umbers (Prichard and Maliotis 1998). The addition of silica, usually in an amorphous form in umbers occurred on the seafloor, is fault controlled and locally pervasive over a few metres (Prichard and Maliotis 1998). Gold concentrations in un-silicified umbers were found to average just 5 ppb whilst silicified umbers contained elevated Au concentrations of up to 5.3 ppm (Prichard and Maliotis 1998).

1. Geological Background

We present four detailed localities that display variable mineralisation styles, all of which are distinctly different from VMS deposits. Whole rock Au concentrations for 10 VMS deposits across Troodos are also presented for comparison (ESM 1, Table S1). Samples presented in this study are divided into VMS deposits and silica-rich mineralisation. The VMS deposits considered span the entire Troodos ophiolite and contain a full suite of ore morphologies, thus, they are representative of a broad range of physicochemical processes (Martin et al. 2019).

Alpen Rose

Alpen Rose forms a prominent NW-SE striking ridge in eastern Troodos, E of the Mathiatis North VMS (Figs. 1 and 2). The mineralisation is situated in the extrusive sequence forming a prominent topographic high, surrounded by 3–10 m wide near vertical dykes that cross-cut sub-horizontal pillow lavas. The ridge is quartz-rich containing a breccia unit cross-cut by quartz veins (Figs. 2 and 3). The southern side of the ridge forms a prominent near vertical scarp that increases in height to the E (Figs. 2 and 3).

Structurally Alpen Rose is complex; a fault bound scarp is present on the southern side delineated by a thick unit of breccia (1–3 m) striking parallel to the ridge (Figs. 2 and 3a,b). Rarely, kinematic indicators are preserved indicating an oblique strike-slip sense of movement (Fig. 2). Local scale N-S strike-slip faults have subsequently cross-cut and offset the entire ridge and adjacent dykes with a displacement of 1–5 m. There is no unified sense of displacement on cross-cutting faults and both sinistral and dextral kinematic indicators are preserved, probably representing fault reactivation under different stress regimes. We infer that Alpen Rose is bound to the SE by a large N-S fault as the ridge and mineralisation end abruptly (Fig. 2).

Mineralisation is dominantly breccia or vein hosted and quartz-rich (Fig. 3e,f). Textures are consistent with multiple phases of sulfide and silica-rich mineralisation. Only minor un-oxidised pyrite was observed at Alpen Rose, however, hematite, goethite and jarosite (cf. section 4.1) that indicate sulfide oxidation are the most abundant matrix-hosted minerals (Fig. 3g,h). Veins are less-common than breccia with a laminated morphology and are typically 30–70 cm wide (Fig. 3c,d).

Mathiatis South

The Mathiatis South deposit has historically been exploited for Au and Cu. It is located SE of the village of Mathiatis (ESM 1, Table S1, Fig. 1) and approximately 2.5 km S of the Mathiatis North VMS. The western margin of the deposit contains a Cu-rich massive pyrite lens (Fig. 4a). The centre of the open pit is dominated by inter-fingered goethite, hematite, jarosite and limonite-rich zones with distinct zones of silica-rich brecciated material (Fig. 4c,h). Brecciation is prolific throughout the entire deposit occurring at a range of scales (Fig. 4b,c,d). In the upper horizon to the east, brecciation becomes less-pronounced instead grading to crudely banded layers (Fig. 4b). Examples of common mineralisation styles are summarised in Fig. 4e–h.

Kokkinovounaros

Kokkinovounaros (Red Hill) forms a prominent topographic high 2 km SW of Analiontas (ESM 1, Table S1, Fig. 1). Mineralisation is bound to the E and W by two parallel N-S striking and eastward dipping normal faults (Fig. 5, see map in ESM 2, Fig. S1). Mineralisation is traceable along strike for ~500 m and is truncated and offset to the S by a NE trending fault. Mineralisation is spatially associated with the N-S faulting with a clear decrease in alteration intensity with distance from the fault plane (~5 m) (Fig. 5a,b). The fault plane is characterised by highly bleached and brecciated lavas with alteration intensity decreasing rapidly from the fault plane to a red-pink zone of jarosite and hematite to a goethite-rich zone at the margins (Fig. 5b).

Brecciation is common throughout Kokkinovounaros with hematite-silica (jasper-rich) breccias occurring proximal to the main N-S fault. Alteration of pyrite is observed as relict cubic pyrite voids now infilled with hematite residue (Fig. 5d). Two different alteration styles are associated with the N-S bounding faults; a stockwork texture that contains disseminated subhedral pyrite (Fig. 5c) and a massive jasper breccia (Fig. 5f–h). Distally from the faults, alteration becomes more chaotic with inter-fingered reds, yellows, whites and pinks indicating variable amounts of hematite, goethite, silica and jarosite respectively. Locally, silicified umber is observed in the hanging wall of faults (Fig. 5e)

Touronjia

Touronjia is located 3.5 km ESE of Kato Lefkara (Fig. 1 and Fig. 6a, ESM 1, Table S1). Silica-sulfide mineralisation occurs in basal group lithologies and grades upwards into LPL flows and brecciated pillows that are directly overlain by the Lefkara limestones (see ESM 2, Fig. S2 for summary map). In the lower regions, sinuous crudely sheeted dykes are highly oxidised grading upwards into a bleached gossanous, silica-rich zone where both silicification and minor kaolinisation occur (Fig. 6b–f). Mineralisation is characterised by pervasive silicification of dykes and pillow lavas accompanied by disseminated pyrite, minor chalcopyrite and covellite with a brecciated texture (Fig. 6c,g,h; ESM 2, Fig. S3). Sulfides are associated with silicification in the matrix of breccia units where pyrite is subhedral and occurs as sub mm scale aggregates and disseminations (ESM 2, Fig. S3).

In the uppermost-mineralised horizon, silicification is pervasive and breccia fragments are hosted in a silica-kaolinite matrix with variable amounts of goethite (Fig. 6a,e,f). In the lower regions, mineralisation is less-pervasively silicified and lavas are identifiable (Fig. 6e,f). Veins of goethite, hematite and silica occur cross-cutting oxidised, but not pervasively altered lavas and no fresh sulfide is observed (Fig. 6f).

Troodos VMS deposits

Whole rock geochemical data for 10 VMS deposits are presented and samples were classified based on their sulfide abundance and morphology into: Massive (n = 17), semi-massive (n = 9), disseminated (n = 9), jasper (n = 11), stockwork (n = 8), South Apliki Breccia Zone (SABZ) (n = 5), ochre (n = 7) and gossan samples (n = 4) (Fig. 7). Massive sulfide contains >90% sulfide, mainly pyrite with minor (<5%) chalcopyrite and trace sphalerite (<1%) (Fig. 7a). Semi-massive samples contain <50% sulfide with a higher silica content (Fig. 7b). Disseminated samples contain fine-grained pyrite (10–20%) but predominantly consist of altered wall-rock (Fig. 7c). Jasper samples contain only pyrite (10–20%), hematite and silica (amorphous or quartz; Fig. 7d). Stockwork samples are characterised by discrete veins of pyrite and chalcopyrite (Fig. 7e). South Apiliki Breccia Zone samples contain high concentrations of chalcopyrite (up to 50%) and variable amounts of covellite, hematite, pyrite and silica (Fig. 7f; Martin et al. 2018). Ochre samples are finely laminated and contain goethite, jarosite and minor hematite (Fig. 7g). Gossan samples are typically goethite-rich with a box-work texture (Fig. 7h).

Methods

Whole rock geochemistry was prepared using an aqua regia digest followed by inductively coupled plasma-mass spectrometry (ICP-MS) analysis. Samples were first crushed using a steel jaw crusher followed by pulverisation in a tungsten carbide TEMA mill. Half a gram of sample was then digested using aqua regia (3:1 HCl:HNO_3). 3.75 ml of HCl and 1.25 ml of HNO_3 was added to the powdered sample and left for 1 hour at room temperature for the initial reaction to subside. Samples where then heated at 85°C for 24 hours and left to cool for 1 hour. A 1:5 dilution was then performed using MilliQ® 18.2 MΩ de-ionised water ready for analysis. Quantitative trace element analysis was performed at Cardiff University using a Thermo iCAP RQ ICP-MS and data correction was performed using the Thermo Qtegra software. Standards UM1, CCU1 and SU1A were prepared in the same dilute aqua regia matrix as the unknown samples, RSD values for Au were better than 1.7% (ESM 1, Table S2 and S3). We acknowledge that aqua regia digestion is not capable of total digestion of silicates; therefore, the Au concentrations presented in this study represent minimum values.

For the identification and quantification of modal mineralogy, X-ray diffraction (XRD) analysis was carried out on powdered samples at Cardiff University. Scans were run using the Philips PW1710 Automated Powder Diffractometer using Cu Kα radiation at 35 kV and 40 mA. From the scans, phases were identified using Philips PC Identify software and from the peak areas, semi-quantitative analysis was performed and a percentage of each phase present was estimated.

Results

Mineralogy

Modal mineralogy analysed by XRD is summarised in Figure 8. Minerals identified include quartz, cristobalite and amorphous silica, multiple Fe phases including goethite (FeO[OH]), jarosite ($KFe^{3+}_3[OH]_6[SO_4]_2$), hematite (Fe_2O_3), carphosiderite ($H_2O•Fe_3[SO_4]_2[OH]_5H_2O$) and other minerals including: natroalunite ($NaAl_3[SO_4]_2[OH]_6$), anatase (TiO_2), sergeevite ($Ca_2Mg_{11}[CO_3]_9[HCO_3]_4[OH_4•6H_2O]$), calcite ($CaCO_3$) and kaolinite ($Al_2SiO_2O_5[OH_4]$) (see Fig. 8 and ESM 2, Fig. S4). Quartz is the most common mineral occurring in 19 out of 24 of samples analysed, its abundance varies significantly from ~5 vol.% to 99 vol.%. Samples from Mathiatis South are the most mineralogically diverse whilst all other deposits analysed contain predominantly quartz with minor goethite, hematite (Alpen Rose) and kaolinite (Touronjia). Based on XRD analysis and hand specimen mineralogy we divide samples from Kokkinovounaros and Mathiatis South into Si-rich, that contain amorphous silica or quartz with only minor hematite and goethite and Fe-rich samples that contain predominantly goethite, hematite and jarosite with lesser amounts of silica. Full data is available in ESM 2, Fig. S4.

Geochemistry

Of the 166 samples analysed from silica-rich mineralisation, 25 returned Au concentrations >1 ppm, with the highest concentration of 20.43 ppm recorded at Mathiatis South (Fig. 9). Median Au concentrations, independent of sample mineralogy are 0.02, 0.38, 0.08 and 0.61 ppm (n = 166; ESM 1, Table S3) for Alpen Rose, Mathiatis South, Kokkinovounaros and Touronjia, respectively (Fig. 9). Samples analysed from Mathiatis South and Kokkinovounaros are sub-divided in Fe- and Si-rich subsets reflecting sample mineralogy (cf. section 4.1).

Of the 48 samples analysed from Mathiatis South, 15 represent Si-rich mineralisation and 33 are Fe-rich. Gold is notably enriched in Si-rich samples with a median concentration of 1.50 ppm (n = 15) compared to 0.24 ppm (n = 33) in Fe-rich samples. Silica-rich samples also exhibit an enrichment in Sb, Ag and Pb and a depletion in Fe, Se, Te, Zn and As relative to Fe-rich samples (Fig. 9). Au does not exhibit any notable correlation in Si-rich samples with the exception of silica (R >0.5) (ESM 1, Table S4). Other notable correlations in Si-rich samples include a strong positive correlation between Fe, As and Se (R >0.8). No notable correlation (R <0.3) exists between Au and other elements analysed in Fe-rich samples (ESM 1, Table S4).

At Kokkinovounaros, of the 59 samples analysed, 11 are classified as Si-rich and 48 are Fe-rich. Au is enriched in Si-rich samples with a median concentration of 1.40 ppm (n = 11) compared to 0.06 ppm (n=48) in Fe-rich samples (Fig. 9; ESM 1, Table S3). Si-rich samples are highly enriched in Pb and Ag with median concentrations of 8.7 and 68.4 ppm compared to Fe-rich samples at 0.4 and 16.6 ppm, respectively (Fig. 9). Fe-rich samples contained elevated concentrations of Zn, Cu, As and Mn relative to Si-rich samples. In Si-rich samples a moderate positive correlation (R >0.4) exists between Au, Mo and Se whereas As and Ag have a strong positive correlation (R = 0.78; ESM 1, Table S4). A moderate negative correlation is recorded between Au and Si (R = -0.6). In Fe-rich samples, correlation with Au is limited with the exception of a minor positive correlation between Au, Ag and Sb (R>0.3) (ESM 1, Table S4).

Samples at Alpen Rose contain the lowest median Au concentration at 0.02 ppm (n = 53) with only one sample containing >1 ppm Au. Alpen Rose samples are enriched in Mn and Co relative to all other Si-rich mineralisation (ESM 1, Table S3). Notably, Au exhibits a moderate positive correlation with Fe (R = 0.65), whereas in all other deposits, Au and Fe exhibit no correlation (R = <0.1). Additionally, a moderate correlation (R >0.6) is recorded between Au with Ag, As, Sb and Bi (ESM 1, Table S4).

Samples from Touronjia contain median Au concentrations of 0.61 ppm (n = 6; Fig. 9). Au exhibits a moderate negative correlation with Si, Fe, Zn, Cu and Cd (R = >-0.6) and a positive correlation with As (R = 0.77; ESM 1, Table S4).

The Au content of VMS samples is highly variable, the highest median Au concentration of 0.26 ppm (n = 9) occurs in semi-massive samples followed by ochre at 0.24 ppm (n = 7) (ESM 1, Table S5). Jasper, stockwork and disseminated mineralization contained the lowest median Au concentration of 0.02 ppm (n = 28). Ochres are enriched in most trace elements relative to massive sulfide samples and contain the highest concentration of Mn, Co, Zn, Se, Ag and Pb (Fig. 9; ESM 1, Table S5). Correlations between Au and As, Ag, Sb and Bi are highly variable. Au exhibits a moderate to strong positive correlation with As, Ag, Sb and Bi in disseminated samples (R = 0.6–0.9; ESM 1, Table S6). The opposite trend is true for ochre samples with a negative correlation between Au, Sb, Bi and As (R = -0.2 to -0.7). See ESM 1, Table S6 for further correlation matrices.

Discussion

Gold in the Troodos hydrothermal system

Gold is associated with both seafloor and subaerial supergene weathering products of VMS deposits such as gossans and ochres (Herzig et al. 1991) and hypogene mineralisation such as sphalerite-rich white smoker vents (Gamo et al. 1996; Maslennikov et al. 2017; Urabe and Kusakabe 1990). Mineralogical characterisation of samples in this study identified two distinct sample suites, namely Fe- and Si-rich samples (section 4.1 and 4.2). We suggest that the mineralogical and geochemical differences between Fe- and Si-rich samples represent subaerial supergene and seafloor hypogene processes. Supergene samples contain high concentrations of goethite, jarosite and hematite (e.g., MAT 39, MAT 36; Fig. 8), common alteration minerals produced by the weathering of sulfide (Herzig et al. 1991), minerals that are notably less-abundant in Si-rich hypogene mineralisation (e.g., MAT 3, KKNV 52; Fig. 8).

At Kokkinovounaros, hypogene mineralisation consists of massive jasper (quartz + hematite) breccias that occur between two N-S trending faults, whilst at Mathiatis South silica-rich samples occur as discrete silicified pods proximal to massive sulfide. In both instances, the morphology and close spatial association of silicified samples with seafloor faulting and massive sulfide suggest a seafloor origin. In contrast, the distribution of supergene alteration at Kokkinovounaros and Mathiatis South is widespread showing limited spatial correlation with faults and a decrease in alteration intensity with increasing stratigraphic depth from the exposed weathering surface, further supporting a subaerial supergene origin.

The enrichment pattern of Au differs between supergene and hypogene samples. At Kokkinovounaros median Au concentrations are 1.4 and 0.1 ppm (n = 59) for hypogene and supergene samples, respectively. A similar distribution is observed between samples at Mathiatis South where hypogene samples contain median concentrations of 1.5 ppm, whilst supergene samples contain only 0.2 ppm Au (n = 48). Furthermore, at both localities the highest Au concentrations correspond to hypogene samples. Thus, the enrichment of Au in silica-rich samples indicates a seafloor origin for Au in silica-rich mineralisation.

In addition to the enrichment of Au in hypogene samples at Kokkinovounaros and Mathiatis South, geochemical distinctions can be made between hypogene and supergene mineralisation, for example, Ag and Pb are enriched in hypogene samples relative to supergene samples (Fig. 9). In contrast, supergene samples may be enriched in As, Se, Cu and Sb, indicating that these metals were primarily hosted in sulfide minerals (Martin et al. 2019) or were preferentially adsorbed onto Fe(oxy)hydroxides during sulfide oxidation (Balistrieri and Chao 1987; Mamindy-Pajany et al. 2009).

The geochemical signatures of Troodos massive sulfides and hypogene silica-rich samples also differ. VMS samples are depleted in Au relative to hypogene samples from Kokkinovounaros, Mathiatis South and Touronjia (Fig. 9). Additionally, VMS samples are enriched in Cu relative to silica-rich mineralisation with median Cu concentrations across all VMS sample types of 933 ppm (n = 70). The difference in geochemistry between massive sulfide samples and silica-rich mineralisation can be explained by affinity of certain metals to high-temperature (~350°C) and sulfide-rich systems. For example, Cu in stockwork samples (Galley et al. 2007) or the enrichment of intermediate to high-temperature elements such as Bi, Mo, Se, Co and Te in VMS deposit (Keith et al. 2016; Monecke et al. 2016; Fig. 9). Our data indicates higher median concentrations of Bi, Se, Co, Mo and Te in VMS samples relative to hypogene silica-rich samples, suggesting that silica-rich mineralisation formed at lower temperatures (ESM 1, Table S3). This is supported by an enrichment of low-temperature elements such as Pb, Sb and Au in silica-rich mineralisation relative to Troodos VMS deposits (Huston and Large 1989; Monecke et al. 2016).

The occurrence of low-temperature fluid venting in Troodos is further supported by fluid inclusion studies at Touronjia (Naden et al. 2006). Mean homogenization temperatures of quartz hosted fluid inclusions at Touronjia were 209°C supporting the occurrence of low-temperature fluid circulation. Additionally, we apply sphalerite geothermometry (Keith et al. 2014; Scott and Barnes, 1971) to the previously published data of Adamides (2013). The application of sphalerite Fe/Zn ratios in this study to data of Adamides (2013) for a Zn-rich prospect located south of Mitsero yield average precipitation temperatures of 246°C (min = 230°C, max = 273°C, n = 14), supporting the occurrence of lower-temperature fluid circulation in Troodos. Hannington et al. (1998) also described a bi-modal distribution in sphalerite Fe content in Troodos VMS, possibly indicating the presence of both high- and low-temperature fluids. These low-temperature fluids contrast those typical for a Troodos VMS with Keith et al. (2016) reporting average precipitation temperatures of 411°C derived from sphalerite at the Skouriotissa VMS. These data indicate that both high-temperature black smoker (>300°C; Von Damm 1995) and lower-temperature (<275°C) hydrothermal activity was present during seafloor spreading.

Low-temperature fluid discharge sites in active hydrothermal fields associated with VMS deposits are reported as localised features. For example, the Kremlin area of the TAG mound that is approximately 20–50 m in diameter and situated <100 m from high-temperature black smoker vents (Tivey et al. 1995). Increased silica abundance, similar to that observed in hypogene samples from Kokkinovounaros and Mathiatis South and in Touronjia samples is also documented for active white smoker vents with amorphous silica and barite intergrown with pyrite and sphalerite (Koski et al. 1984; Tivey et al. 1995). Similar textural and mineralogical associations have been described for the extinct MESO vent site(s) in the central Indian Ocean that are characterised by jasper breccias that formed at temperatures of <265°C (Halbach et al. 2002). Similar mineralogical associations are documented in Troodos silica-rich mineralisation, for example at Kokkinovounaros where elevated Au concentrations are associated with jasper-rich breccias (Fig. 5f–h). In combination, temperatures derived from sphalerite geothermometry (Adamides 2013), fluid inclusion analysis (Naden et al. 2006) and indirectly from mineralogical and geochemical variations between VMS deposits and silica-rich mineralisation in this study, indicate different chemical and physical fluid properties between these hydrothermal systems. Fluids responsible for forming silica-rich mineralisation were low-temperature <300˚C, Au-rich and in some instances where hematite forms the dominant Fe mineral, fluids were locally more oxidising.

Previous studies at Touronjia by Naden et al. (2006) suggest a possible magmatic volatile source for Au; similar to processes associated with subaerial epithermal type mineralisation (White and Hedenquist 1990). This observation is primarily based on the occurrence of kaolinite and dickite as key alteration minerals indicating low pH fluids (White and Hedenquist 1990). In their proposed model, Au and associated elements such as Bi, Te and Se are sourced from the direct contribution of a magmatic volatile phase (cf. Yang and Scott 1996; de Ronde et al. 2005). If this was the case then an enrichment in these elements is expected at Touronjia and this is not observed with median concentrations of 0.02 ppm Bi, 0.11 ppm Te and 1.34 ppm Se (n = 6; ESM 1, Table S3). Additionally, fluid inclusion data presented by Naden et al. (2006) yield average salinities close to modern seawater (~3.5 wt.% NaCl) suggesting fluids of seawater and not magmatic origin (i.e. brines or vapour), supporting a low-temperature seawater origin.

Mineralisation at Alpen Rose shares many similar attributes with other localities e.g. abundant silicification and brecciation, yet Alpen Rose is depleted in Au compared to other silica-rich mineralisation (median = 0.02 ppm Au, n = 53). We suggest that local-scale permeability variations coupled with a high-temperature fluid source explain this depletion. Gold at Alpen Rose was probably associated with sulfide-rich mineralisation as it exhibits a moderate positive correlation (R = >0.5) with Pb, Te, Ag, Mo and Fe (ESM 1, Table S4); in all other silica-rich mineralisation a negative correlation with Fe is observed. At Alpen Rose, goethite and hematite are abundant and occur in the matrix of breccias representing the supergene oxidisation of pyrite during weathering. Additionally, a small enrichment in Co at Alpen Rose relative to massive sulfide samples and other silica-rich mineralisation could represent a high-temperature fluid source (Keith et al. 2016) with a similar trace element composition to VMS stockwork samples, excluding Cu that is relatively depleted at Alpen Rose (Fig. 9). We infer that the geochemical signature preserved at Alpen Rose is indicative of high-temperature fluids that were not affected by later low-temperature off-axis fluid flow and therefore contain low Au concentrations (Fig. 10) (Patten et al. 2016).

This hypothesis is supported by field observations at Alpen Rose that indicate that the majority of quartz formed early in the deposit paragenesis as it predates sulfide (now goethite-hematite) mineralisation that forms the matrix of breccias (Fig. 3g,h). Initial quartz brecciation occurred during a period of increased fault movement that led to a localised increase in permeability facilitating a high-temperature fluid pulse and sulfide precipitation (Fig. 10). The precipitation of sulfides occluded initial permeability pathways, effectively sealing the Alpen Rose hydrothermal system from later, low-temperature silica- and Au-rich fluids (Fig. 10). These late stage low-temperature fluids were channelled through the nearby Mathiatis North VMS where late Au-rich quartz veins cross-cut massive sulfide (Martin et al. 2019). This indicates that Au and silicification post-date VMS formation, as demonstrated by Prichard and Maliotis (1998) for silicified umbers. Therefore, the low Au concentrations at Alpen Rose can be explained by i) the timing of silicification and quartz formation relative to fault movement, ii) the high-temperature, probably near axis location of Alpen Rose, and iii) sulfide precipitation leading to the occlusion of late-stage fluid pathways (Fig. 10).

Models for gold enrichment

Silica-rich mineralisation at Troodos is comparable to a variety of modern day sites of effusive, low-temperature venting that occur within the VMS mound as white smokers or off-axis as sites of effusive fluid discharge ("shimmering water") (Gamo et al. 1996; Halbach et al. 2002; Hannington et al. 1991). Silica-rich mineralisation in Troodos share many similar attributes with seafloor hosted low-temperature vent sites, including: i) abundant silica and silicification, ii) mineralisation that occurs distally to high-temperature VMS deposits, iii) an enrichment in Au and, iv) indirect mineralogical and geochemical evidence of low-temperature fluids <300˚C.

Gold in the Troodos ophiolite was initially mobilised during high-temperature (>350˚C) fluid-rock interaction within the SDC, as epidosite zones that form a source region for some metals in Troodos VMS deposits are depleted in Au (Patten et al. 2017). Upwelling high-temperature, metal-rich fluids undergo mixing with shallow, lower temperature, oxidised seawater-derived fluids at the basal-group-LPL boundary (Alt 1994, 1995). Mixing between down-welling seawater and up-welling hydrothermal fluid within this transitional zone facilitates the precipitation of secondary pyrite that incorporates trace metals (Alt 1994; Alt and Teagle 2003). Disseminated pyrite is widely observed throughout the basal-group-LPL transition in Troodos, most notably in areas such as Almyras and Mosfiloti (Fig. 11).

Secondary disseminated sulfide probably formed at temperatures <250°C as celadonite and chalcedony are the dominant alteration minerals present in the LPL stratigraphy of Troodos (Alt 1994; Gass and Smewing 1973). Disseminated sulfide formed at, or within close proximity to the spreading axis and would have been coeval with high-temperature hydrothermal systems that formed in areas of focused fluid discharge associated with graben bounding faults and VMS deposit formation (Fig. 11). The associated change in redox and decrease in temperature during the diffuse mixing of hydrothermal and seawater derived fluids within the basal-group in a "near axis" position provides an trapping mechanism for Au and other trace metals incorporated into disseminated sulfides (Fig. 11; Alt 1994). In the shallow subsurface in the low-temperature alteration zone (UPL) temperatures were cooler (120–200°C; Pedersen et al., 2017) and pyrite formation by biogenic sulfate reduction could have occurred, however the extent of this process in Troodos is poorly constrained (Alt and Shanks 2011; Pedersen et al. 2017). Patten et al. (2016) document elevated concentrations of Au, As, Sb and Se in sulfides at the transitional zone between the SDC and overlying pillow lavas in Hole 1256D (Cocos Plate). They suggested that the mixing of hydrothermal fluids with seawater at this horizon acted as a sink for trace metals that were mobilised during epidosite formation and the alteration of the SDC below (Patten et al. 2016).

As the crust migrated further from the ridge axis, heat and fluid flux from the underlying SDC decreased whereas the amount of seawater influx remained high leading to a decrease in fluid temperature distally (km’s to 10’s of km) from the spreading axis (Alt 1995; Alt and Teagle 2003). In contrast to high-temperature on-axis VMS forming fluids, the cooler off-axis fluids (<250˚C) effectively scavenged and remobilised metals that have an increased affinity for lower-temperature fluids such as Au, Zn, Pb and Sb (Monecke et al., 2016) from basal group sulfides, earlier formed VMS deposits and epidosite zones (Fig. 11; Hannington et al., 1986). Au was transport as sulfide or bi-sulfide complexes more efficiently in these lower-temperature fluids (Pokrovski et al. 2014; Williams-Jones et al. 2009). Low Au concentrations at Alpen Rose and VMS deposits in Troodos are attributed to the decreased solubility of Au at high-temperatures (~350˚C) where neither Cl^- nor HS^- complexes effectively transport Au (Hannington and Scott 1989; Pokrovski et al. 2014; Williams-Jones and Heinrich 2005; Williams-Jones et al. 2009). We propose that Touronjia, Kokkinovounaros and Alpen Rose represent an intermediary (~250˚C?) between a typical high-temperature (>350˚C) VMS deposit and the ultra-low temperature <100°C (?) silicification of umbers (Fig. 11) (Prichard and Maliotis 1998).

Alternate processes where Au is enriched through the addition of a magmatic volatile phase have been suggested for bi-modal VMS environments (Patten et al. 2019; Sun et al. 2004; Yang and Scott 1996). However, our data provides little evidence of magmatic dominated fluids in silica-rich mineralisation, for example, the lack of an advanced argillic alteration assemblage (e.g., natroalunite, pyrophyllite and native sulfur) that indicate low pH, magmatic, volatile-rich fluids (de Ronde et al. 2019; Herzig et al. 1998). We also suggest that if a magmatic volatile influx did occur in Troodos it would have been limited to high-temperature hydrothermal systems in an on-axis position and the initial stages of VMS formation and not off-axis regions (Martin et al. 2020).

At Mathiatis South, Au enrichment reflects local-scale processes related to zone refining and mound-scale fluid flow and not the remobilisation of Au during off-axis fluid flow. At Mathiatis South, Au was remobilised from the high-temperature inner core zone of the VMS mound towards the cooler mound margins during zone refining (Galley et al. 2007), resulting in the simultaneous venting of black and white smoker fluids (Fig. 11). Similar vents occur in active seafloor systems such as the Kremlin area of the TAG mound (Humphris et al. 1995; Petersen et al. 2000). In contrast to Mathiatis

South, all other mineralisation is located distally to known VMS deposits and does not reflect mound-scale remobilisation processes. If this were the case then Au would not demonstrate a clear association with quartz veins that cross-cut and postdate VMS deposits, for example at the Mathiatis North VMS (Martin et al. 2019).

Further detailed investigation to quantify and validate the proposed model should include the detailed petrographic and geochemical analysis of sulfides and oxides from the basal group transition. This should be complimented by sulfur isotope analysis ($\delta^{34}S$) of sulfides in silica-rich mineralisation to elucidate a magmatic volatile source of metals in the off-axis hydrothermal system.

Structural implications

All low-temperature silica-rich mineralisation investigated in this study is structurally controlled and occurs within the eastern portion of the Troodos ophiolite in a complex region known as the Makheras domain (Varga and Moores 1985). The Makheras domain is bound by the Larnaca graben to the E and the Mitsero graben to the W. Throughout the area, NW-SE and N-S faulting is observed. The intersection of these two fault directions appears to be important in controlling the distribution of Au and silicification in off-axis mineralisation.

Low-temperature silica-rich mineralisation is spatially associated with either normal or strike-slip faulting. The Makheras structural domain (cf. Varga and Moores 1985) exhibits cross-cutting relationships consistent with multiple, temporally distinct faulting and hydrothermal events. For example, at Alpen Rose where NW-SE trending faults and dykes are cross-cut by strike-slip N-S trending faults. This suggests that axial parallel (Larnaca) NW-SE faults were cross-cut by later re-activated faults associated with the N-S orientated Mitsero graben. The interplay between these two structural regimes relates to the migration of spreading between different ridge axes that led to localised dilation, reactivation and propagation of new faults aligned to the developing stress regime. Renewed faulting in older, cooler, more permeable crust by late stage cross-cutting faults likely acted as a conduit channelling late-stage silicifying fluids (Prichard and Maliotis 1998) and similar cross-cutting fault regimes have been identified at Touronjia and Kokkinovounaros.

Summary and Conclusions

Silica-rich mineralisation forms an intermediary between on-axis VMS deposits and low-temperature silicification of umbers. Geochemical data identify an enrichment in Au at Kokkinovounaros, Mathiatis South and Touronjia relative to Troodos VMS deposits. Zones of silica-rich mineralisation at these locations share common attributes including their geochemistry, abundant quartz or amorphous silica and their location distal to sites of high-temperature venting. We draw parallels between low-temperature silica-rich mineralisation in Troodos and active white smoker or effusive type vents on the modern seafloor. Low-temperature deposits of the Troodos ophiolite are variably enriched in Au, Sb, Pb and Zn relative to Troodos VMS. This enrichment reflects the enhanced solubility of these metals in low-temperature fluids that were generated during the migration of crust away from the spreading axis.

As the crust migrated away from the spreading axis fluids became progressively cooler. These lower temperature fluids transported Au more effectively as sulfide and bi-sulfide complexes. We suggest that Au was scavenged and remobilised from basal group sulfides or epidosite zones. These Au-rich fluids were then channelled along reactivated faults at graben margins concentrating off-axis fluid flow leading to the formation of Au and silica-rich mineralisation.

Acknowledgments

The authors acknowledge the support of the Geological Survey Department of Cyprus, especially Costas Costantinou and Andreas Zissimos. We thank Michael Green, Lazaros Georgiou and Ifigenia Gavriel for discussion and assistance in the field. Anthony Oldroyd is thanked for his assistance during XRD analysis. This research was funded by the NERC SoS consortium grant NE/M010848/1 “TeaSe: tellurium and selenium cycling and supply” awarded to Cardiff University. We thank Clifford Patten and an anonymous reviewer for their comments that greatly improved this manuscript. We also thank associate editor Thomas Monecke and the editor-in-chief Georges Beaudoin for the efficient editorial handling of the manuscript. We dedicated this manuscript to the late Hazel M. Prichard.

References

Adamides N (2010) Mafic-dominated volcanogenic sulphide deposits in the Troodos ophiolite, Cyprus Part 2- A review of genetic models and guides for exploration. Appl Earth Sci 119:193–204

Adamides NG (2013) South Mathiatis: An unusual volcanogenic sulphide deposit in the Troodos ophiolite of Cyprus. Appl Earth Sci 122:194–206

Alt JC (1994) A sulfur isotopic profile through the Troodos ophiolite, Cyprus: Primary composition and the effects of seawater hydrothermal alteration. Geochim Cosmochim Acta 58:1825–1840

Alt JC (1995) Subseafloor processes in mid-ocean ridge hydrothermal systems. Geophys Monogr, Am Geophys Union 91:85–85

Alt JC, Honnorez J, (1984) Alteration of the upper oceanic crust, DSDP site 417: mineralogy and chemistry. Contrib to Mineral Petr 87:149–169

Alt JC, Shanks WC(2011) Microbial sulfate reduction and the sulfur budget for a complete section of altered oceanic basalts, IODP Hole 1256D (eastern Pacific). Earth Planet Sci Lett 310, 73–83

Alt JC, Teagle DA (2003) Hydrothermal alteration of upper oceanic crust formed at a fast-spreading ridge: mineral, chemical, and isotopic evidence from ODP Site 801. Chem Geol 201: 191–211

Balistrieri LS, Chao TT (1987) Selenium adsorption by goethite. Soil Sci Soc Am 51:1145–1151

Constantinou G, Govett GJS (1973) Geology, geochemistry, and genesis of Cyprus sulfide deposits. Econ Geol 68:843–858

Cook NJ, Ciobanu CL, Pring A, Skinner W, Shimizu M, Danyushevsky L, Saini-Eidukat B, Melcher F (2009) Trace and minor elements in sphalerite: A LA-ICPMS study. Geochim Cosmochim Acta 73:4761–4791

de Ronde CEJ, Hannington MD, Stoffers P, Wright IC, Ditchburn RG, Reyes AG, Baker ET, Massoth GJ, Lupton JE, Walker SL, Greene RR, Soong CWR, Ishibashi J, Lebon GT, Bray CJ, Resing JA (2005) Evolution of a Submarine Magmatic-Hydrothermal System: Brothers Volcano, Southern Kermadec Arc, New Zealand. Econ Geol 100:1097–1133

de Ronde CE, Humphris SE, Höfig TW, Reyes AG, IODP Expedition 376 Scientists (2019) Critical role of caldera collapse in the formation of seafloor mineralization: The case of Brothers volcano. Geology 47:762–766

Escartín J, Canales JP (2011) Detachments in oceanic lithosphere: Deformation, magmatism, fluid flow, and ecosystems. Eos, Trans Am Geoph Union 92:31–31

Galley AG, Hannington MD Jonasson IR, (2007) Volcanogenic massive sulphide deposits. Mineral deposits of Canada: A synthesis of major deposit-types, district metallogeny, the evolution of geological provinces, and exploration methods: Geol Ass of Canada, Min Dep Division, Spec Pub 5:141–161

Gamo T, Chiba H, Masuda H, Edmonds HN, Fujioka K, Kodama Y, Nanba H, Sano Y (1996) Chemical characteristics of hydrothermal fluids from the TAG Mound of the Mid-Atlantic Ridge in August 1994: Implications for spatial and temporal variability of hydrothermal activity. Geophys Res Lett 23:3483–3486

Gass IG (1968) Is the Troodos Massif of Cyprus a Fragment of Mesozoic Ocean Floor? Nature 220:39–42

Gass IG (1980) The Troodos massif: Its role in the unravelling of the ophiolite problem and its significance in the understanding of constructive plate margin processes, in: Ophiolites, Proceedings: International Ophiolite Symposium, Cyprus 1979. The Geological Survey Department, Ministry of Agriculture and Natural Resources, Nicosia, Cyprus, 23–35

Gass IG, Smewing JD (1973) Intrusion, Extrusion and Metamorphism at Constructive Margins: Evidence from the Troodos Massif, Cyprus. Nature 242:26–29

Halbach M, Halbach P, Lüders V (2002) Sulfide-impregnated and pure silica precipitates of hydrothermal origin from the Central Indian Ocean. Chem Geol 182:357–375

Hannington MD, Scott SD (1989) Sulfidation equilibria as guides to gold mineralization in volcanogenic massive sulfides; evidence from sulfide mineralogy and the composition of sphalerite. Econ Geol 84:1978–1995

Hannington MD, Peter JM, Scott SD (1986) Gold in sea-floor polymetallic sulfide deposits. Econ Geol 81:1867–1883

Hannington M, Herzig P, Scott S, Thompson G, Rona P (1991) Comparative mineralogy and geochemistry of gold-bearing sulfide deposits on the mid-ocean ridges. Mar Geol, Cenozoic Geology of the Nortwest European Continental Margin and Adjacent Deep-Sea Areas 101: 217–248

Hannington M, Jonasson I, Herzig P, Petersen S (1995) Physical and Chemical Processes of Seafloor Mineralization at Mid Ocean Ridges. Wash. DC Am Geophys Union Geophys Monogr Ser 91:115–157

Hannington MD, Galley A, Herzig P, Petersen S (1998) Comparison of the TAG mound and stockwork complex with Cyprus-type massive sulfide deposits. Proc Ocean Drill Program Sci Results 158:389–415

Heinrich CA, Driesner T, Stefánsson A, Seward TM (2004) Magmatic vapor contraction and the transport of gold from the porphyry environment to epithermal ore deposits. Geology 32:761–764

Herzig PM, Hannington MD, Scott SD, Maliotis G, Rona PA, Thompson G (1991) Gold-rich sea-floor gossans in the Troodos Ophiolite and on the Mid-Atlantic Ridge. Econ Geol 86:1747–1755

Herzig PM, Hannington MD, Arribas Jr A (1998) Sulfur isotopic composition of hydrothermal precipitates from the Lau back-arc: implications for magmatic contributions to seafloor hydrothermal systems. Minera Deposita 33:226–237

Honnorez J, Von Herzen RP, Barrett TJ, Becker K, Bender ML, Borella PE, Hubberten HW, Jones SC, Karato SI, Laverne C, Levi S (1981) Hydrothermal mounds and young ocean crust of the Galapagos: Preliminary Deep Sea Drilling results, Leg 70. Geol Soc of Am Bull 92:457–472

Humphris SE, Herzig PM, Miller DJ, Alt JC, Becker K, Brown D, Brügmann G, Chiba H, Fouquet Y, Gemmell JB, Guerin G, Hannington MD, Holm NG, Honnorez JJ, Iturrino GJ, Knott R, Ludwig R, Nakamura K, Petersen S, Reysenbach A-L, Rona PA, Smith S, Sturz AA, Tivey MK, Zhao X (1995) The internal structure of an active sea-floor massive sulphide deposit. Nature 377:713–716

Hurst SD, Moores EM, Varga RJ (1994) Structural and geophysical expression of the Solea graben, Troodos Ophiolite, Cyprus. Tectonics 13:139–156

Huston DL, Large RR (1989) A chemical model for the concentration of gold in volcanogenic massive sulphide deposits. Ore Geol Rev 4:171–200

Jowitt SM, Jenkin GRT, Coogan LA, Naden J (2012) Quantifying the release of base metals from source rocks for volcanogenic massive sulfide deposits: Effects of protolith composition and alteration mineralogy. J Geochem Explor 118:47–59

Keith M, Haase KM, Schwarz-Schampera U, Klemd R, Petersen S, Bach W (2014) Effects of temperature, sulfur, and oxygen fugacity on the composition of sphalerite from submarine hydrothermal vents. Geology 42:699-702

Keith M, Haase KM, Klemd R, Krumm S, Strauss H (2016) Systematic variations of trace element and sulfur isotope compositions in pyrite with stratigraphic depth in the Skouriotissa volcanic-hosted massive sulfide deposit, Troodos ophiolite, Cyprus. Chem Geol 423:7–18

Koski RA, Clague DA, Oudin E (1984) Mineralogy and chemistry of massive sulfide deposits from the Juan de Fuca Ridge. GSA Bull 95:930–945

Mamindy-Pajany Y, Hurel C, Marmier N, Roméo M, (2009). Arsenic adsorption onto hematite and goethite. C R Chim 12:8 876-881

Martin AJ, McDonald I, MacLeod CJ, Prichard HM, McFall K (2018) Extreme enrichment of selenium in the Apliki Cyprus-type VMS deposit, Troodos, Cyprus. Mineralogical Magazine 82:697–724

Martin AJ, Keith M, McDonald I, Haase KM, McFall KA, Klemd R, MacLeod CJ (2019) Trace element systematics and ore-forming processes in mafic VMS deposits: Evidence from the Troodos ophiolite, Cyprus. Ore Geol Rev 106:205–225

Martin, AJ, Keith M, Parvaz DB, McDonald I, Boyce AJ, McFall KA, Jenkin GR, Strauss H, MacLeod, CJ (2020) Effects of magmatic volatile influx in mafic VMS hydrothermal systems: Evidence from the Troodos ophiolite, Cyprus. Chem Geol 531:119–325

Maslennikov VV, Maslennikova SP, Large RR, Danyushevsky LV, Herrington RJ, Ayupova NR, Zaykov VV, Lein AY, Tseluyko AS, Melekestseva IY, Tessalina SG (2017) Chimneys in Paleozoic massive sulfide mounds of the Urals VMS deposits: Mineral and trace element comparison with modern black, grey, white and clear smokers. Ore Geol Rev 85: 64–106

Melekestseva IY, Maslennikov VV, Tret'yakov GA, Nimis P, Beltenev VE, Rozhdestvenskaya II, Maslennikova SP, Belogub EV, Danyushevsky L, Large R, Yuminov AM, Sadykov SA (2017) Gold- and Silver-Rich Massive Sulfides from the Semenov-2 Hydrothermal Field, 13°31.13'N, Mid-Atlantic Ridge: A Case of Magmatic Contribution? Econ Geol 112:741–773

Mercier-Langevin P, Hannington MD, Dubé B, Bécu V (2011) The gold content of volcanogenic massive sulfide deposits. Miner Deposita 46:509–539

Miyashiro A (1973) The Troodos ophiolitic complex was probably formed in an island arc. Earth Planet Sci Lett 19, 218–224

Monecke T, Petersen S, Hannington MD, Grant H, Samson I (2016) The minor element endowment of modern sea-floor massive sulfides and comparison with deposits hosted in ancient volcanic successions. Rev Econ Geol 18:245–306.

Moss R, Scott SD (2001) Geochemistry and Mineralogy of Gold-Rich Hydrothermal Precipitates from the Eastern Manus Basin, Papua New Guinea. Can Mineral 39:957–978

Mukasa SB, Ludden JN (1987) Uranium-lead isotopic ages of plagiogranites from the Troodos ophiolite, Cyprus, and their tectonic significance. Geology 15:825–828

Naden J, Herrington RJ, Jowitt SM, Mcevoy FM, Williamson JP, Monhemius AJ (2006) New methodologies for volcanic-hosted copper sulphide mineralization on Cyprus: A GIS-prospectivity analysis-based approach. BGS Int Rep CR/06/129:241

Patten CGC, Pitcairn IK, Teagle DAH, Harris M (2016) Mobility of Au and related elements during the hydrothermal alteration of the oceanic crust: implications for the sources of metals in VMS deposits. Miner Deposita 51:179–200

Patten CGC, Pitcairn IK, Teagle DAH (2017) Hydrothermal mobilisation of Au and other metals in supra-subduction oceanic crust: Insights from the Troodos ophiolite. Ore Geol Rev 86:487–508

Patten CGC, Pitcairn IK, Alt JC, Zack T, Lahaye Y, Teagle DAH, Markdahl K (2019) Metal fluxes during magmatic degassing in the oceanic crust: sulfide mineralisation at ODP site 786B, Izu-Bonin forearc. Miner Deposita 1-21

Pearce JA, Robinson PT (2010) The Troodos ophiolitic complex probably formed in a subduction initiation, slab edge setting. Gondwana Res 18:60–81

Pedersen LER, Staudigel H, McLoughlin N, Whitehouse MJ, Strauss H (2017) A multiple sulfur isotope study through the volcanic section of the Troodos ophiolite. Chem Geol 468: 49–62

Petersen S, Herzig PM, Hannington MD (2000) Third dimension of a presently forming VMS deposit: TAG hydrothermal mound, Mid-Atlantic Ridge, 26°N. Miner Deposita 35:233–259

Pokrovski GS, Akinfiev NN, Borisova AY, Zotov AV, Kouzmanov K (2014) Gold speciation and transport in geological fluids: insights from experiments and physical-chemical modeling. Geol Soc Lond Spec Publ 402:9-70

Prichard HM, Maliotis G (1998) Gold mineralization associated with low-temperature, off-axis, fluid activity in the Troodos ophiolite, Cyprus. J Geol Soc 155:223–231

Schoonen MA, Fisher NS, Wente M (1992) Gold sorption onto pyrite and goethite: A radiotracer study. Geochim Cosmochim Acta 5:1801-1814

Scott SD,Barnes HL (1971) Sphalerite geothermometry and geobarometry. Econ Geol 66:653-669

Sun W, Arculus RJ, Kamenetsky VS, Binns RA (2004) Release of gold-bearing fluids in convergent margin magmas prompted by magnetite crystallization. Nature 431:975–978

Tivey MK, Humphris SE, Thompson G, Hannington MD, Rona PA (1995) Deducing patterns of fluid flow and mixing within the TAG active hydrothermal mound using mineralogical and geochemical data. J Geophys Res Solid Earth 100:12527–12555

Urabe T, Kusakabe M (1990) Barite silica chimneys from the Sumisu Rift, Izu-Bonin Arc: possible analog to hematitic chert associated with Kuroko deposits. Earth Planet Sci Lett 100:283–290

van Everdingen DA, Cawood PA (1995) Dyke domains in the Mitsero graben, Troodos ophiolite, Cyprus: an off-axis model for graben formation at a spreading centre. J Geol Soc 152:923–932

Varga RJ, Moores EM (1985) Spreading structure of the Troodos ophiolite, Cyprus. Geology 13:846–850

Von Damm KL (1995) Controls on the chemistry and temporal variability of seafloor hydrothermal fluids. Seafloor hydrothermal systems: Physical, chemical, biological, and geological interactions, 91:222–247

White NC, Hedenquist JW (1990) Epithermal environments and styles of mineralization: Variations and their causes, and guidelines for exploration. J Geochem Explor 36:445–474

Williams-Jones AE, Heinrich CA (2005) Vapor transport of metals and the formation of magmatic-hydrothermal ore deposits. Econ Geol 100:1287–1312

Williams-Jones AE, Bowell RJ, Migdisov AA (2009) Gold in Solution. Elements 5:281–287

Yang, K., Scott, S.D. (1996) Possible contribution of a metal-rich magmatic fluid to a sea-floor hydrothermal system. Nature 383:420–423

Figure Captions

Figure 1: Simplified geological map of the Late Cretaceous (92 Ma) Troodos ophiolite, Cyprus. Black dashed lines indicate the approximate location of graben axes. Green circles are VMS deposits and orange triangles are silica-rich mineralisation (after Martin et al. 2019).

Figure 2: Geological map of the Alpen Rose. Where faults are intersected, quartz and sulfide (now Fe-oxide) abundance increases. The surrounding extrusive sequence is cross-cut by a series of dyke swarms (parallel to Alpen Rose) that are truncated by strike-slip faults, indicating that N-S faults postdate NW-SE faulting. Yellow letters identify photo localities presented in Fig. 3. See text for further discussion.

Figure 3: Field photographs from Alpen Rose. A) View looking SE from the base of Alpen Rose. Alpen Rose forms a prominent topographic high. B) View looking NW; note the prominent steep sided fault scarp delineating the main breccia zone. C) Top of the main ridge, a massive quartz vein is offset by minor dextral strike-slip faults. D) Quartz breccia vein with silica cement. E and F) Angular quartz clasts in a hydrothermally altered weakly silicified matrix. G and H) Typical hydrothermal "sulfide-rich" breccia. White clasts are sub-angular quartz in a goethite-hematite matrix.

Figure 4: Field photographs from Mathiatis South. A) View over the historic open pit, note extensive oxidisation and acid mine lake. B) Typical gossan exposure, interlayered goethite, jarosite and hematite. C) Silica breccia from the main pit exposure. D) Layered gossan exposure. E) Silicified lava

containing high Au. F) Typical gossan sample consisting of goethite with minor quartz. G) Calcite-goethite-rich sample, black mineral is Mn carbonate. H) Silica breccia exhibiting a "vuggy silica" texture. Number above hand specimen indicates the Au content of sample. Scale bar in E-H are 1 cm squares.

Figure 5: Field photographs from Kokkinovounaros. A) View of the historic open pit (looking N along main pit fault). Note highly bleached lavas surrounding the fault plane. B) Cross-section of alteration zone surrounding the main pit fault. The fault plane is marked by intense leaching (white) grading through goethite to hematite (orange to red) and finally into "fresh" green-grey pillow lavas. C) Stockwork veins in close proximity to the western fault, inset image shows subhedral pyrite grains in reflected light. D) Supergene altered lava: euhedral voids indicate the leaching of pyrite now containing hematite residue. E) Silicified umber to the S of the main pit exposure. F) Exposure in a small adit to the N of Kokkinovounaros preserving hypogene jasper-rich breccia mineralisation (see ESM 2, Fig. S1). G and H) Examples of high-Au jasper from location F (adit). Number above hand specimen indicates the Au content of sample. Scale bar in G and H are 1 cm squares.

Figure 6: Field photographs from Touronjia. A) View over the mineralised area, the far hill tops are Lefkara group limestones. B) Upper Touronjia exposure, brecciated highly silicified unit with variable amounts of Fe staining. C) Fresh surface of Touronjia breccia, the unit is pervasively silicified with trace sulfides. D) Close-up of clast supported Fe-stained breccia. E and F) Vein hosted "sulfide" mineralisation, now altered to goethite-jarosite cross-cutting an altered lava. G and H) Examples of high Au samples exhibiting a distinct brecciated morphology with a highly silicified matrix commonly containing disseminated sulfide. Number above hand specimen indicates the Au content of sample. Scale bar in G and H are 1 cm squares. See ESM 2, Fig. S2 for photo locations and summary map.

Figure 7: Examples of sample types analysed in Troodos VMS deposits. Samples represent different supergene and hypogene processes synonymous with VMS mineralisation. Stockwork (E) contains chalcopyrite, quartz and pyrite-rich veins. South Apliki Breccia Zone (F) mineralisation consists of a

hematite matrix with large quantities of chalcopyrite, covellite and pyrite. See text for further characterisation.

Figure 8: Modal mineralogy analysed by XRD of samples from Mathiatis South (MAT), Touronjia (TJ), Kokkinovounaros (KKNV) and Alpen Rose (AR) (ESM 2, Fig. S4). Samples from Touronjia, Kokkinovounaros and Alpen Rose are quartz dominated with minor Fe minerals whilst Mathiatis South samples are generally jarosite, goethite and silica-rich (silica*= cristobalite and amorphous phase). Au concentrations of corresponding sample shown above sample in ppm.

Figure 9: Whole-rock geochemistry (aqua regia) for low-temperature, silica-rich mineralisation (dashed boxes) and VMS (dotted boxes) classified by location or sample morphology (in ppm). A) Au, B) Ag, C) As, D) Pb, E) Zn and F) Cu. Element correlation is summarised in ESM 1, Table S4 and S6. Solid boxes represent upper quartile, textured boxes represent lower quartile, and the black line the median concentrations. Minimum and maximum values are represent the whiskers. For full data see ESM 1, Table S3 and S5. For standard information and RSD for all elements, see ESM 1, Table S2. See text for discussion.

Figure 10: The formation of Alpen Rose mineralisation (MN = Mathiatis North VMS, AR = Alpen Rose). **T1**: Alpen Rose forms proximal to the ridge axis from intermediate temperature silica-rich fluids. At this time, the Mathiatis North VMS forms at the ridge axis. **T2**: Fault movement at Alpen Rose increases permeability leading to brecciation of early quartz veins and the venting of high-temperature fluids that leads to the precipitation of sulfide-rich mineralisation. Sulfides occlude fluid flow pathways. **T3**: As the fluid flow at Alpen Rose decreases, late stage off-axis Au- and silica-rich fluids are channelled through the nearby, more permeable Mathiatis North VMS deposit.

Figure 11: Schematic summary of the enrichment of Au in the Troodos hydrothermal system. Au is initially sourced from leaching of metals in the SDC. In close proximity to the ridge axis Au may be enriched in white smoker mineralisation. A) Au in a white smoker type setting e.g. Mathiatis South. The enrichment of Au reflects mound scale fluid flow and Au enrichment is spatially associated with VMS mineralisation. Slightly further off-axis but still within an area of high heat and fluid flux Alpen

Rose mineralisation forms (cf. Fig. 10). B) Au may be sourced through the leaching of metals from VMS deposits. Low-temperature hydrothermal fluid (orange arrows; <250°C) remobilises and scavenges trace metals from sulfides in the VMS mound. C) Diffuse fluid flow from the underlying SDC mixes with circulating seawater leading to the precipitation of disseminated sulfides within the basal-group-LPL stratigraphy (orange arrows). As the fluid flow and heat flux decrease as the crust migrates further off-axis fluid become progressively cooler (<250°C) and metals are scavenged and remobilised from sulfide minerals (mainly pyrite) by lower temperature fluids. Au is transported as sulfide and bi-sulfide complexes. Fluids are then channelled along late-stage reactivated faults leading to the formation of silica-rich Au mineralisation. The silicification of umber occurs distally at temperatures of ~100°C (?) as the crust continued to migrated off-axis and fluids cooled further.

Figure 1

Click here to access/download;Figure;Figure_1_REV.2.jpg

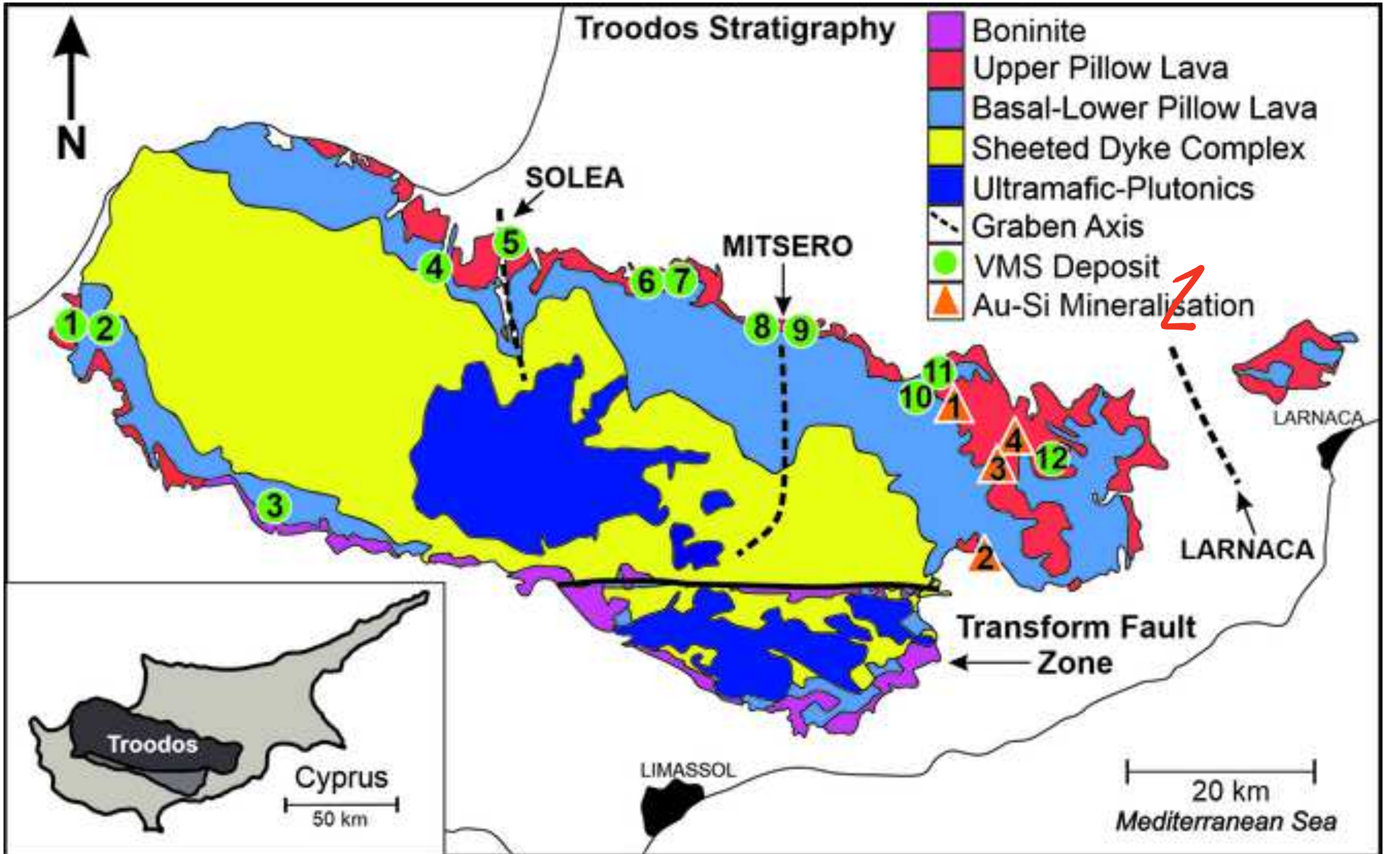

VMS mineralisation

1. Limni
2. Kynousa
3. Mala
4. Apliki
5. Skouriotissa
6. Alestos
7. Memi
8. Kokkinoyia
9. Agrokipia
10. Kaphedes
11. Kambia
12. Sha

Au-Si mineralisation

1. Kokkinovounaros
2. Touronjia
3. Mathiatis South
4. Alpen Rose

*grid ref. provided in ESM 1

add symbol

Figure 2

2 in text

Click here to access/download;Figure;Figure_2_REV.jpg

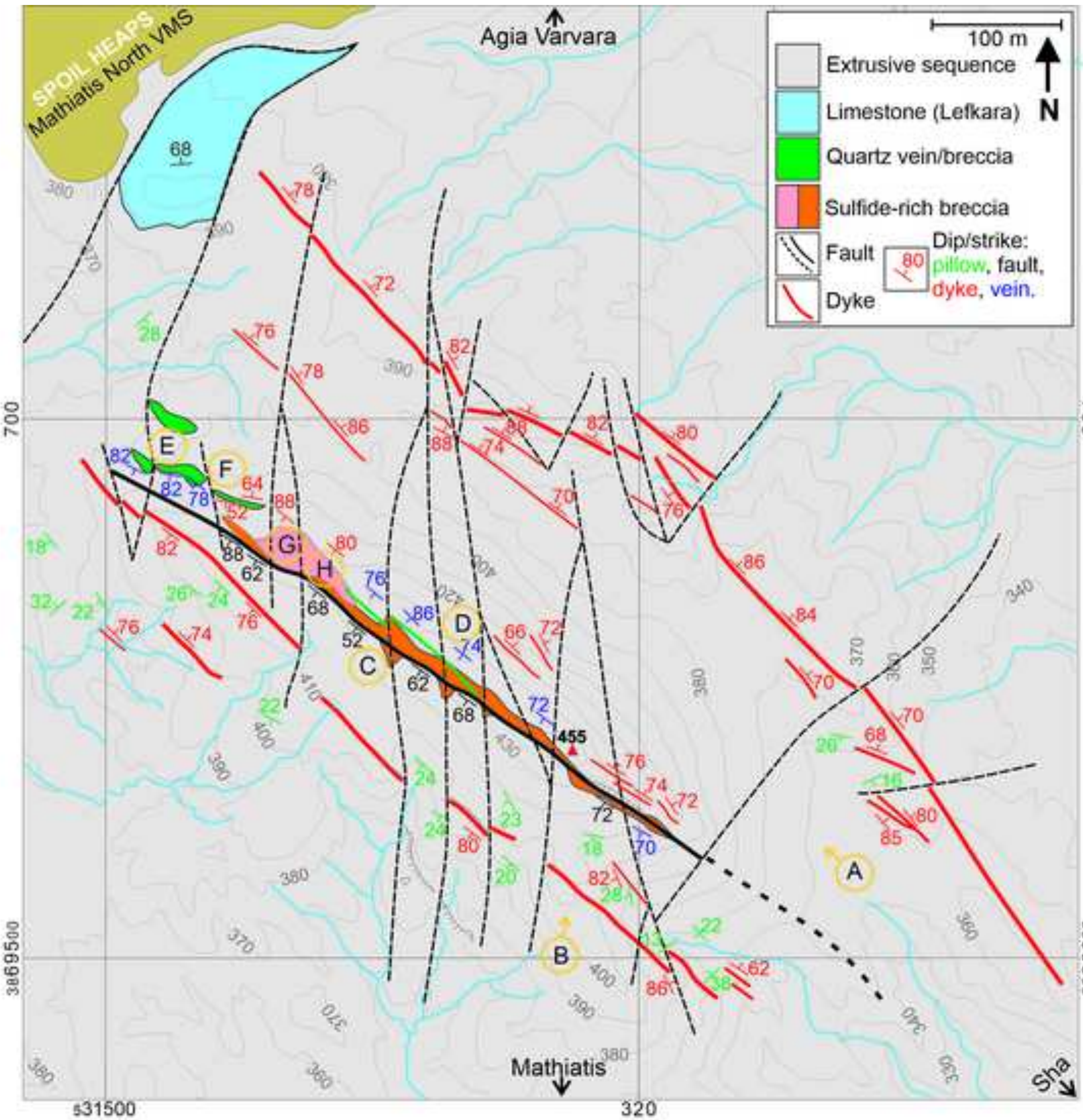

Figure 3

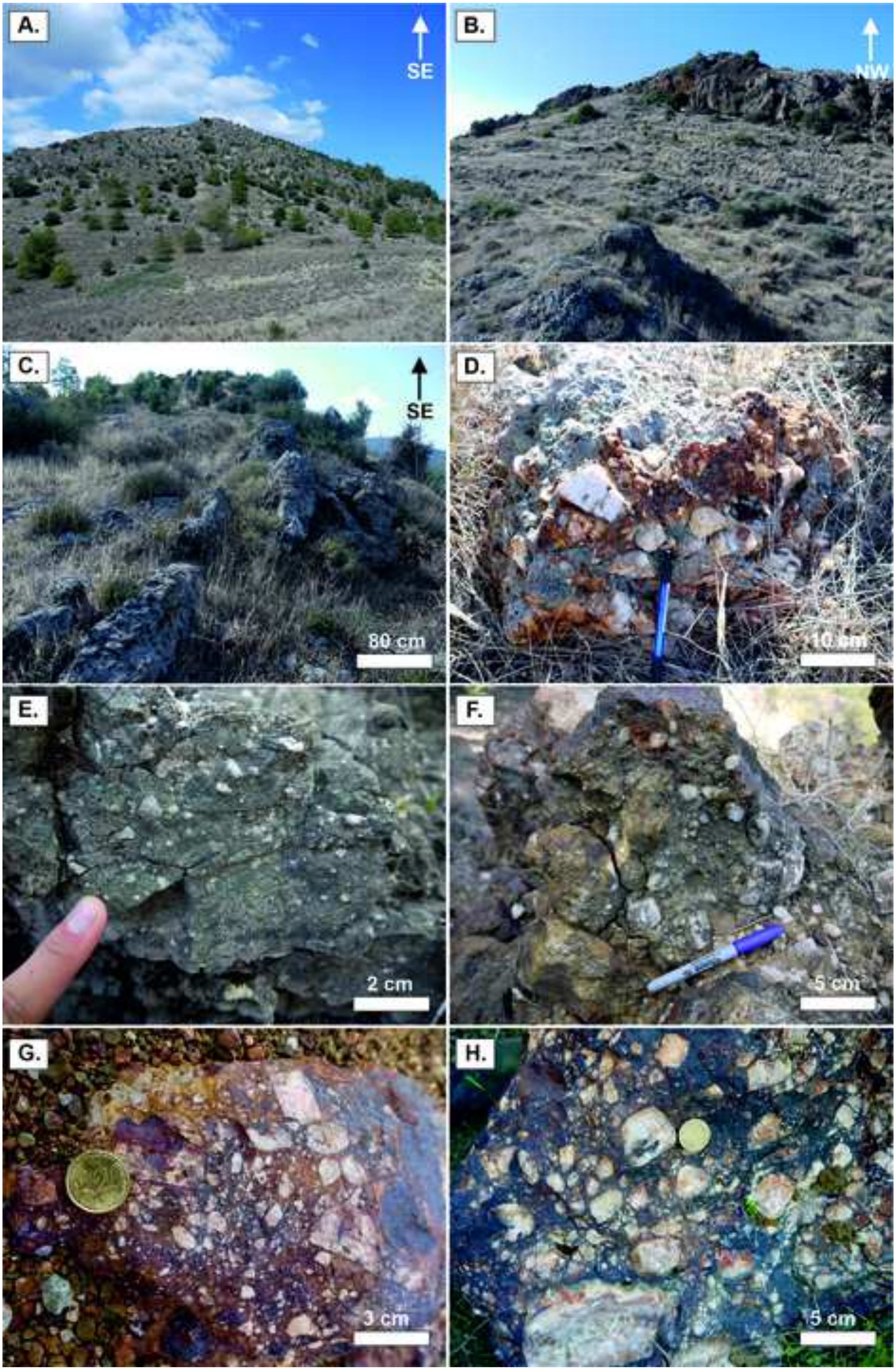

Figure 4

Click here to access/download;Figure;Figure_4_REV.jpg

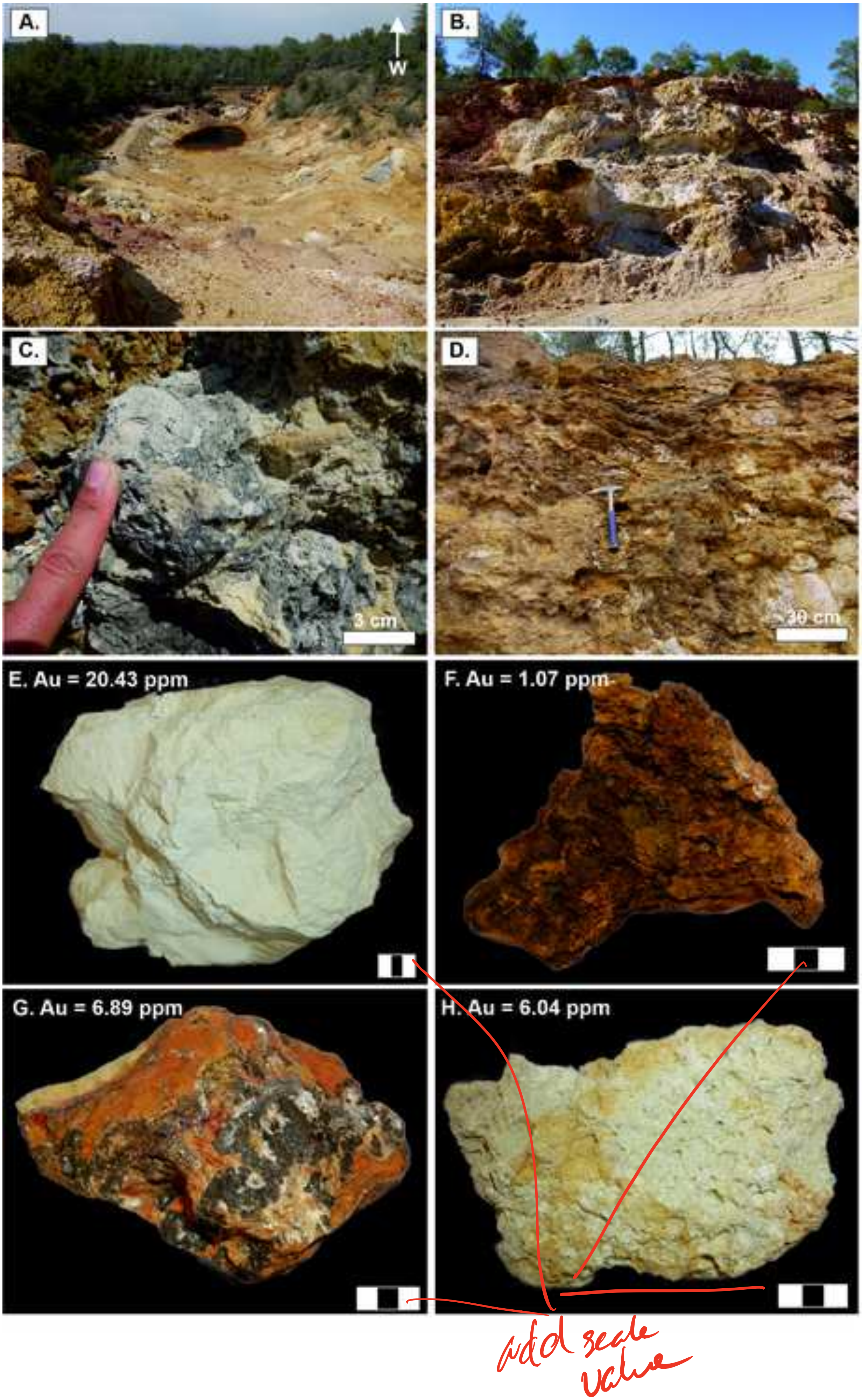

Figure 5

Click here to access/download;Figure;Figure_5_REV.jpg

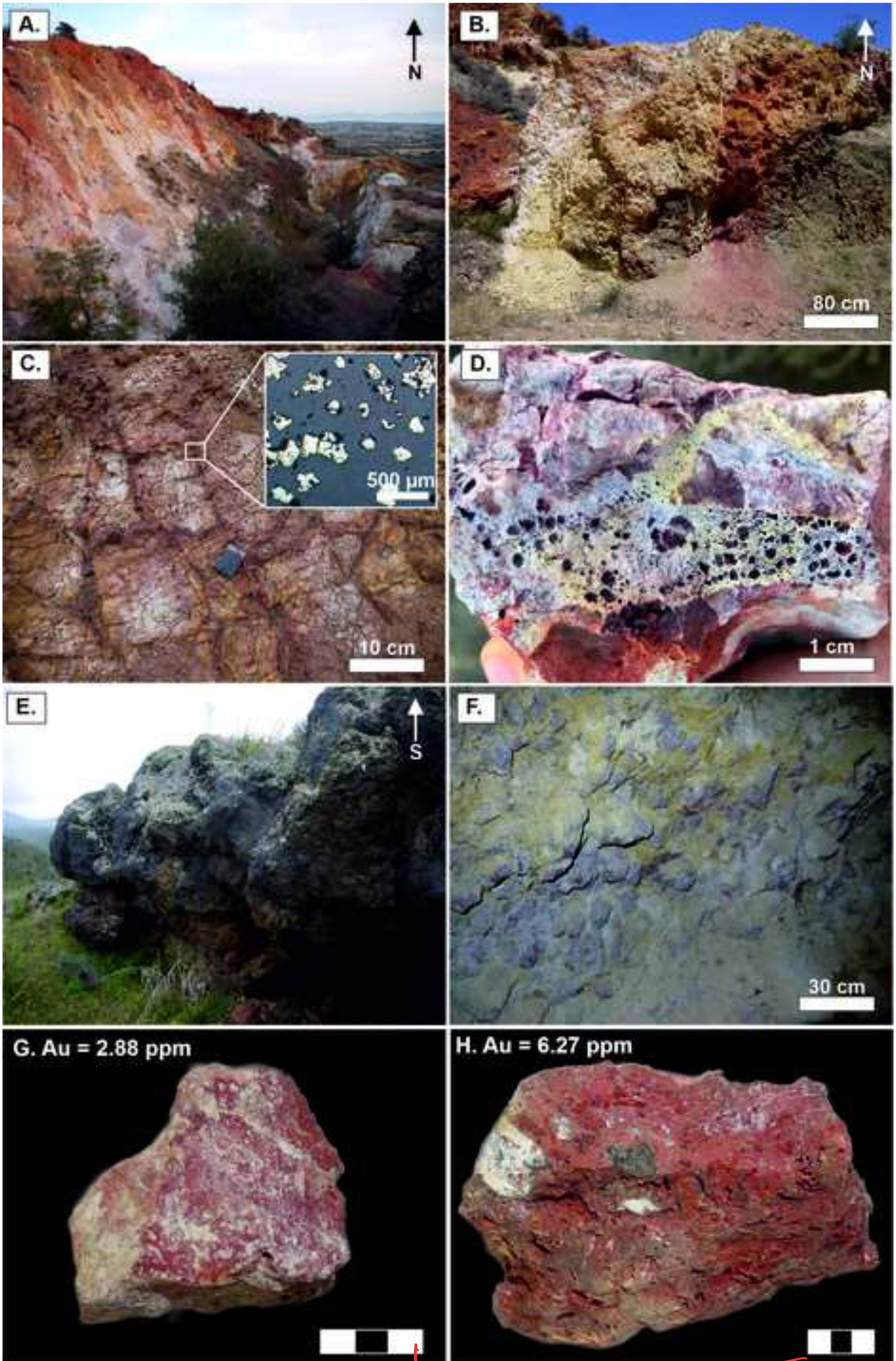

iden scale values

Figure 6

Click here to access/download;Figure;Figure_6_REV.jpg

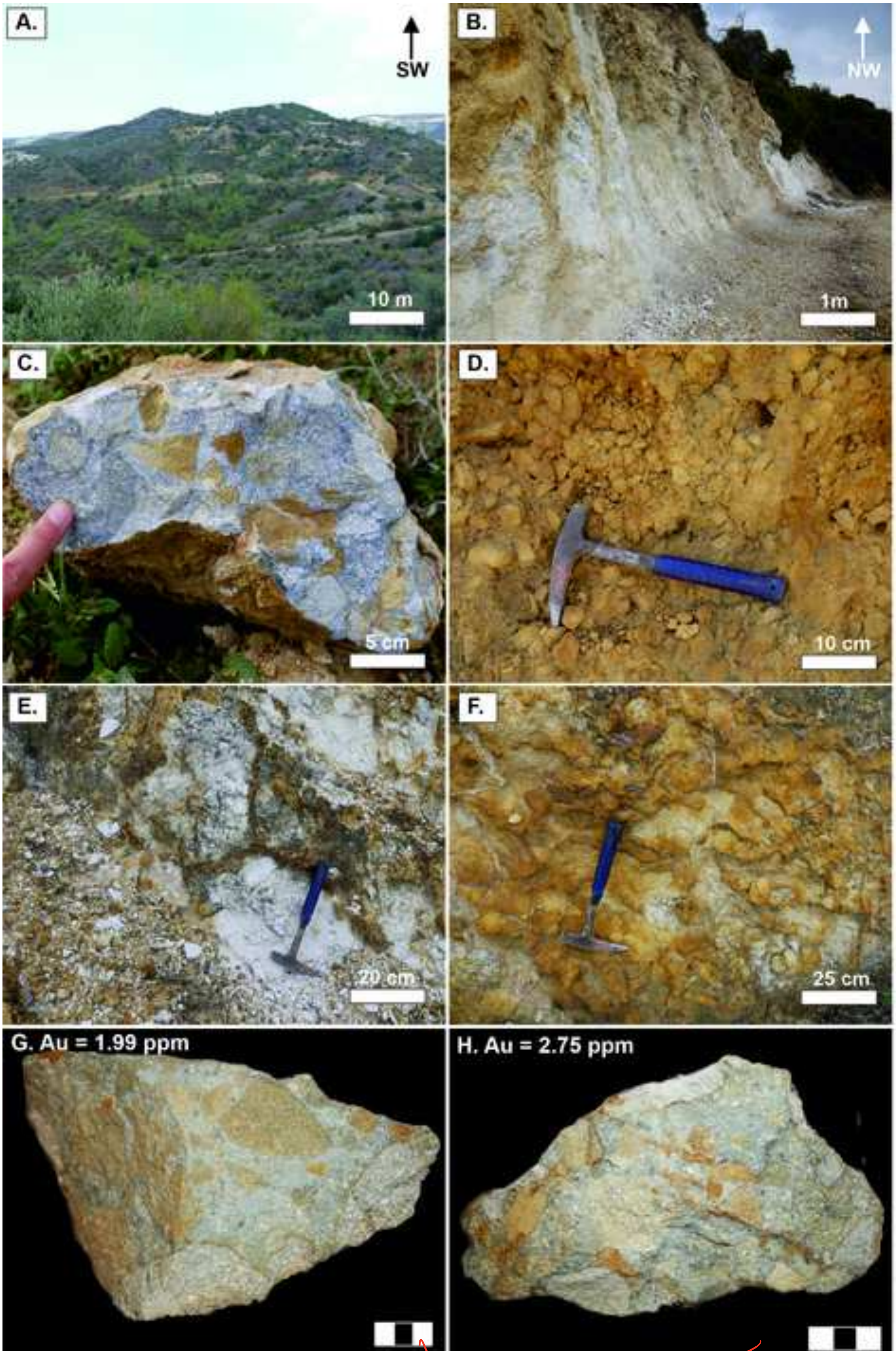

idem add scale values

Figure 7

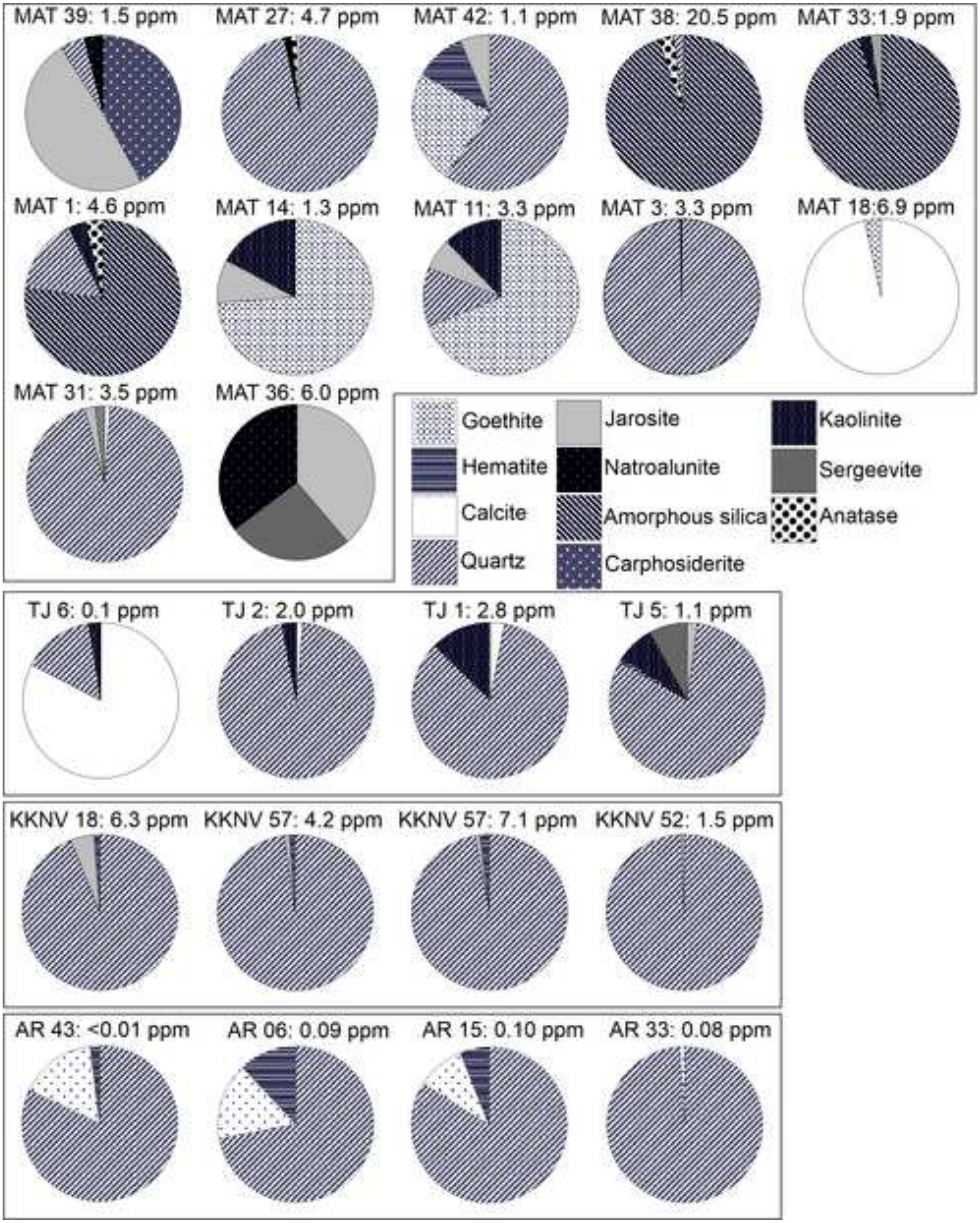
MAT 39: 1.5 ppm
MAT 27: 4.7 ppm
MAT 42: 1.1 ppm
MAT 38: 20.5 ppm
MAT 33:1.9 ppm
MAT 1: 4.6 ppm
MAT 14: 1.3 ppm
MAT 11: 3.3 ppm
MAT 3: 3.3 ppm
MAT 18:6.9 ppm
MAT 31: 3.5 ppm
MAT 36: 6.0 ppm
Goethite
Jarosite
Kaolinite
Hematite
Natroalunite
Sergeevite
Calcite
Amorphous silica
Anatase
Quartz
Carphosiderite
TJ 6: 0.1 ppm
TJ 2: 2.0 ppm
TJ 1: 2.8 ppm
TJ 5: 1.1 ppm
KKNV 18: 6.3 ppm
KKNV 57: 4.2 ppm
KKNV 57: 7.1 ppm
KKNV 52: 1.5 ppm
AR 43: <0.01 ppm
AR 06: 0.09 ppm
AR 15: 0.10 ppm
AR 33: 0.08 ppm


A.
1cm
B.
1cm
C.
1cm
D.
2cm
E.
2cm
F.
1cm
G.
1cm
H.
2cm
Sample types:
A. Massive pyrite
B. Semi-massive pyrite
C. Disseminated
D. Jasper
E. Stockwork
F. SABZ
G. Ochre
H. Gossan

Figure 9

Click here to access/download;Figure;Figure_9_REV.2.jpg

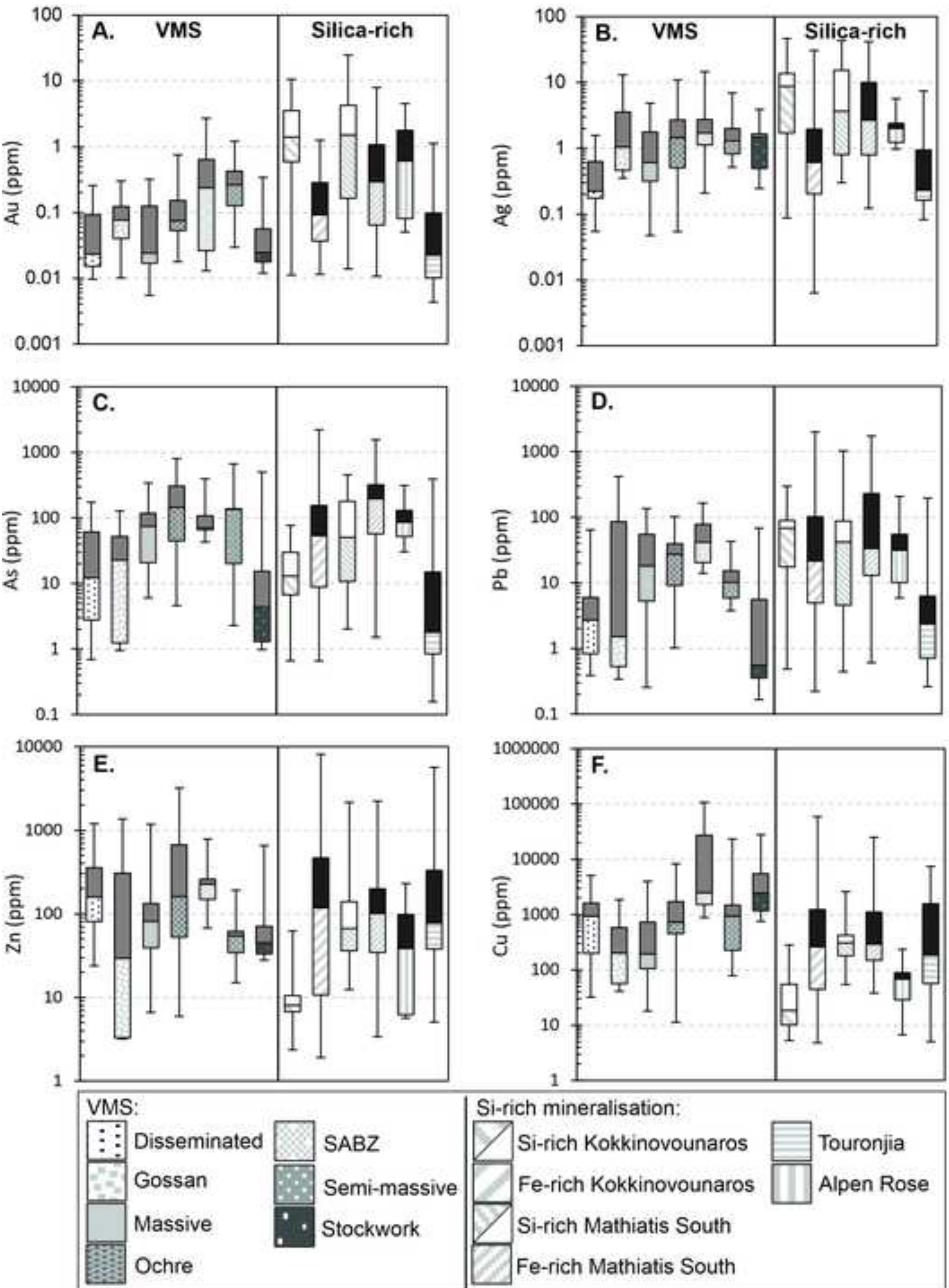

you could use color, nicer and free!

Figure 10

Click here to access/download;Figure;Figure_10_REV.jpg

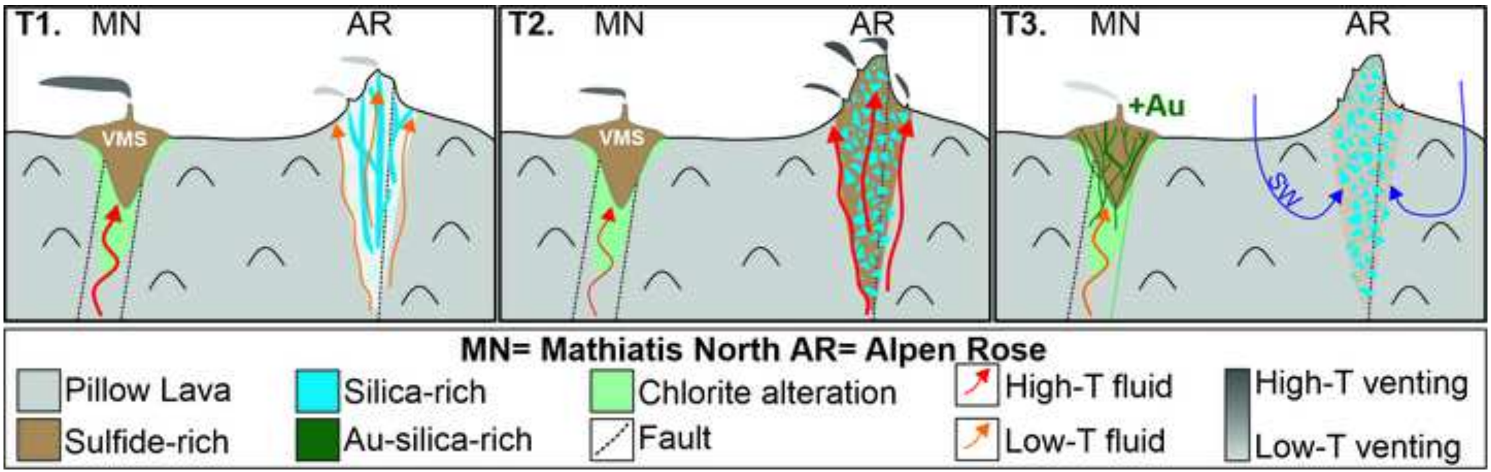

Figure 11

Click here to access/download;Figure;Figure_11_REV.2.jpg